Structural and dynamical heterogeneity of water trapped inside Na^+-pumping KR2 rhodopsin in the dark state

Mantu Santra,[†] Aniruddha Seal,[‡] Kankana Bhattacharjee,[¶] and Suman Chakrabarty[*,¶]

†*School of Chemical and Materials Sciences, Indian Institute of Technology Goa, Ponda, Goa 403401, India*

‡*School of Chemical Sciences, National Institute of Science Education and Research, Bhubaneswar 752050, Odisha, India*

¶*Department of Chemical, Biological & Macro-Molecular Sciences, S. N. Bose National Centre for Basic Sciences, Kolkata 700106, West Bengal, India*

E-mail: sumanc@bose.res.in

Abstract

Photoisomerisation in retinal leads to a channel opening in the rhodopsins that triggers translocation of an ion/proton. Crystal structures of rhodopsins contain several structurally conserved water molecules. It has been suggested that water plays an active role in facilitating the ion pumping/translocation process by acting as a lubricant in these systems. In this work, we investigate the localisation, local structure and dynamics of water molecules along the channel for the resting/dark state of KR2 rhodopsin. Employing 1.5 μs long atomistic molecular dynamics (MD) simulations of this trans-membrane protein system, we demonstrate the presence of five distinct water containing pockets/cavities separated by gateways controlled by the protein side-chains. We present evidence of significant structural and dynamical heterogeneity in the water molecules present in these cavities. The exchange time-scale of these buried water with bulk ranges from tens of nanoseconds to > 1.5 μs. The translational and rotational dynamics of buried water are found to be strongly dependent on protein cavity size and local interactions with possible functional significance.

Introduction

Vision or photo-sensing in living organisms is possible due to the ability of rhodopsins to convert light into electrochemical signal in terms of translocation of ions.[1,2] Rhodopsins belong to the largest group of membrane proteins, namely G protein-coupled receptors (GPCR) that trigger a wide range of signaling pathways in cells and are most promising targets of therapeutics. Until very recently, the rhodopsins were known to function either as inward chloride or outward proton pumps. However, in 2013 the first discovery of a sodium ion (Na^+) pumping rhodopsin (KR2) was made in *Krokinobacter eikastus*.[3–5]

Similar to all microbial rhodopsins, KR2 is a transmembrane protein consisting of seven parallel α-helices that span across the membrane.[4–8] A retinal chromophore is covalently

attached to lysine residue (LYS255) near the central part of the protein which undergoes cis-trans isomerisation upon activation through light and thus controls the ion transport across the cell membrane. KR2 contains a unique Asn-Asp-Gln (NDQ) motif which is used to pump Na^+.[3,9,10] This is in contrast to bacterial rhodopsin (bR) which possesses highly conserved Asp-Thr-Asp (DTD) motif that carries out proton pumping.[11,12] However, in absence of Na^+, KR2 acts as a proton pump.[13] Moreover, a variant of KR2 has been designed which is able to pump K^+ making it a potential optogenetic tool.[4,5,7,14]

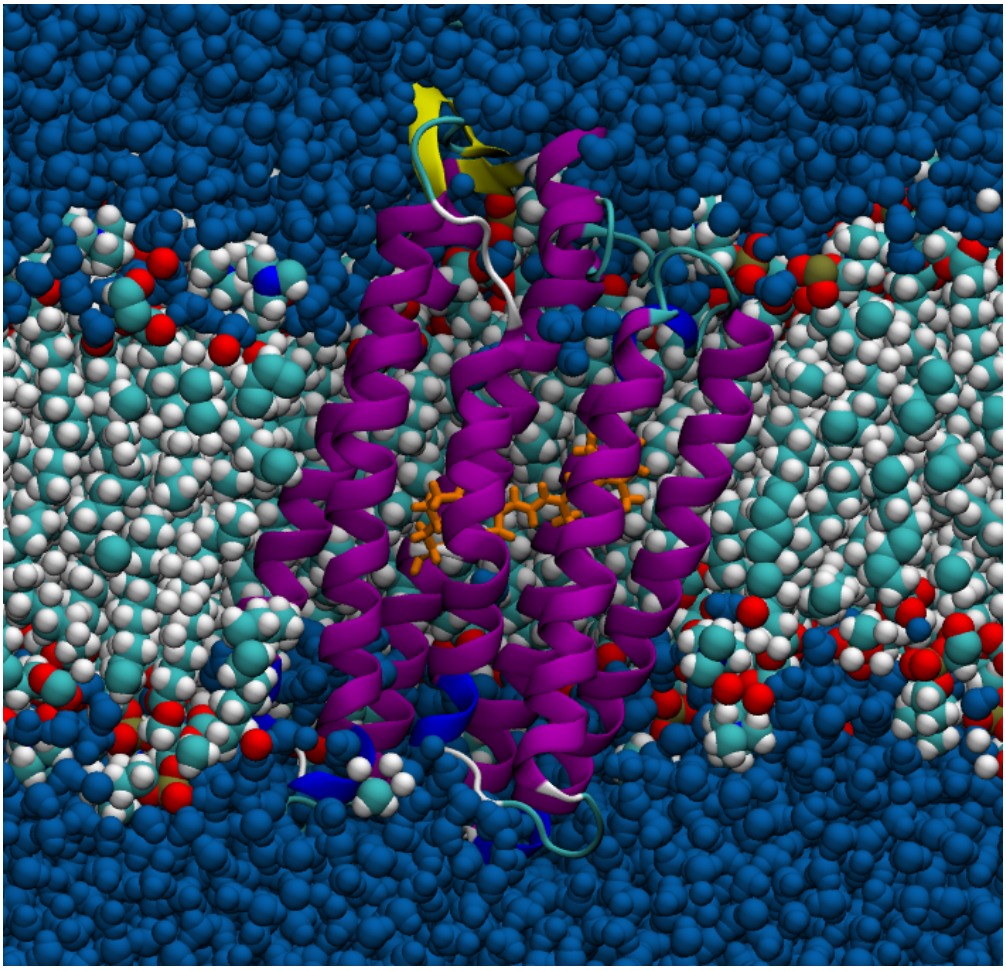

Figure 1: **Simulated system:** The structure of KR2 Rhodopsin in the resting state embedded in a DMPC bilayer with the retinal chromophore being covalently attached to the LYS255 residue at the middle of the channel (highlighted in dark yellow). The retinal is in all-trans conformation here. The protein-membrane system is solvated with water (blue).

The photo-catalytic cycle of all microbial rhodopsins including KR2 consists of four

intermediates. The resting structure of KR2 shows an all-trans retinal chromophore in which the Schiff base is in protonated state. Upon photo-activation, the $C_{13} = C_{14}$ bond undergoes rotation and forms 13-cis isomer (K) followed by formation of L state via conformational changes to the protein. In the next step, the Schiff base is deprotonated and the proton is transferred to the Asp116 forming a blue shifted M state.[3,15] The reprotonation of Schiff base leads to the formation of state O which eventually relaxes back to the resting (KR2) state. According to the experimental evidences, the uptake and release of Na^+ occur in $L/M \rightarrow O$ and $O \rightarrow KR2$, respectively.[2,3,13,16,17]

Interestingly, all GPCR proteins and in particular rhodopsins contain structurally conserved bound water molecules buried deep inside the protein channel. Hence, it has been often suggested that these bound water molecules play a crucial role in the function of these biomolecules.[11,18–23] The crystal structure of KR2 rhodopsin exhibits several such bound water molecules that motivate us to explore the nature of these buried hydration sites, structural and dynamical properties of the water molecules present in these cavities and their possible functional role in terms of coupling with the conformational states of the protein.[6,7,24]

The active role of water in determining the structure, function and dynamics of biomolecular systems has been discussed extensively in literature.[25–36] Binding to or hydration of specific sites influences the functionality and the specificity for proteins and protein-DNA complexes.[37–39] The static and dynamical properties of water bound to surface or interior of a biomolecule can be drastically different from bulk water depending on the local environment.[36,40–44]

Water is a deceptively simple molecule with fascinating chameleon-like adaptibility. Many of its properties are highly context dependent. The structure and dynamics of water may vary depending on whether it is near a hydrophobic/hydrophilic molecule/surface, whether it is under confinement, and even different properties of water are perturbed to different extent depending on the nature of the perturbation.[45,46] For water molecules bound to protein surface or buried inside protein cavities, the residence time may vary over a wide range

depending on the nature of the interactions. ^{17}O and ^{2}H nuclear magnetic relaxation dispersion (NMRD) study by *Denisov et al.*[47] revealed that the exchange time of water bound to protein spans over a broad range of time scale: the water bound to protein surface exchanges in the time scale of 10-50 ps, whereas those bound strongly to the protein show 0.1-1 ns exchange time scale. Water with even slower exchange time scale has been observed by Ernst *et al*[48] in case of human interleukin-1β where they found disordered water molecules trapped into hydrophobic cavities for longer than 1 ns. An extensive theoretical study on the kinetics of water exchange in cytrochrome c by *Garcia et al.* depicts diverse time scales depending on the location of the binding site and the local interaction energies.[49]

Recent theoretical study on the localisation of water inside KR2 rhodopsin channel shows reorganisation of water molecules upon conformational transitions of the protein.[50] Another simulation study on Channelrhodopsin-2 (ChR2) revealed that the water acts as a lubricant in the ion transportation.[19] In addition, the water at the specific sites may play a major role in the ion transport processes.[11,51–53] Therefore, understanding the molecular level structure and dynamics of water will help us to better understand the mechanism of Na^{+} pumps, and rhodopsins in general, which eventually could be used for the rational design of novel light-driven ion pumps and development of inhibitory optogenetic tools.[3,4,54,55]

Given the above background, in this work we have carried out an extensive atomistic molecular dynamics (MD) simulation to understand the localisation, local structure, hydration and dynamics of water inside KR2 channel in the resting (dark) state. Our study identifies several spatially disjoint specific water binding sites and their nature in terms of available space, local interaction and water dynamics. We also investigated the residence time of water molecules in different cavities identified along the channel. We establish a direct connection of our findings with the available experimental data in the KR2 literature.

Computational details

All atom classical molecular dynamics (MD) simulations were carried out using the Gromacs software suite.[56] The simulated system consisted of the trans-membrane protein KR2 from *K. eikastus* (PDB: 3X3B)[4] embedded in DMPC bilayer using the CHARMM-GUI web-server.[57] The protein-membrane system was solvated by water (TIP3P water model) and neutralised by Cl^- ions. Na^+ and Cl^- ions were added to maintain 150 mM concentration of NaCl. The system comprised of 1 protein, 367 DMPC, 80 Na^+, 82 Cl^- and 26,776 water molecules. The total number of atoms was 1,25,000. Periodic Boundary Condition (PBC) has been employed in all directions. See Fig. 1 for a visual representation of the system.

The system was simulated at 310 K temperature and 1 bar pressure using velocity rescaling thermostat[58] and Parrinnello-Rahman semi-isotropic barostat[59] with $2fs$ integration time step. The barostat was coupled separately in xy plane and z-direction. We used the CHARMM36 force field [60] for all the components except the retinal chromophore. The force field for retinal was obtained from the earlier work by Hayashi *et al.*[61–65] The long range electrostatic forces were taken care of by using the particle-mesh Ewald (PME) method. We carried out MD simulation for $1.5\mu s$. The last $1\mu s$ of this trajectory was used for subsequent analyses.

Results and discussion

Identification of cavity and water localisation

Several crystal structures of KR2 contain multiple water molecules along the channel and they have been suggested to be functionally important.[4,7,24] Earlier simulation study on KR2 rhodopsin has shown that even in the resting state water molecules may be continuously distributed along the channel forming two clusters separated at the vicinity of the retinal.[50] In this work, discrete positions of water molecules at different time frames were superimposed

to visually identify the clusters. Instead of that, in order to generate a more refined statistical measure of the water distribution, we have computed the spatial density of water along the channel. The spatial density has been computed by averaging the local densities (in three dimensional grids) along the channel over the $1\mu s$ long MD trajectory. The density of water clearly shows five distinct pockets/cavities (I-V) along the channel (Fig. 2).

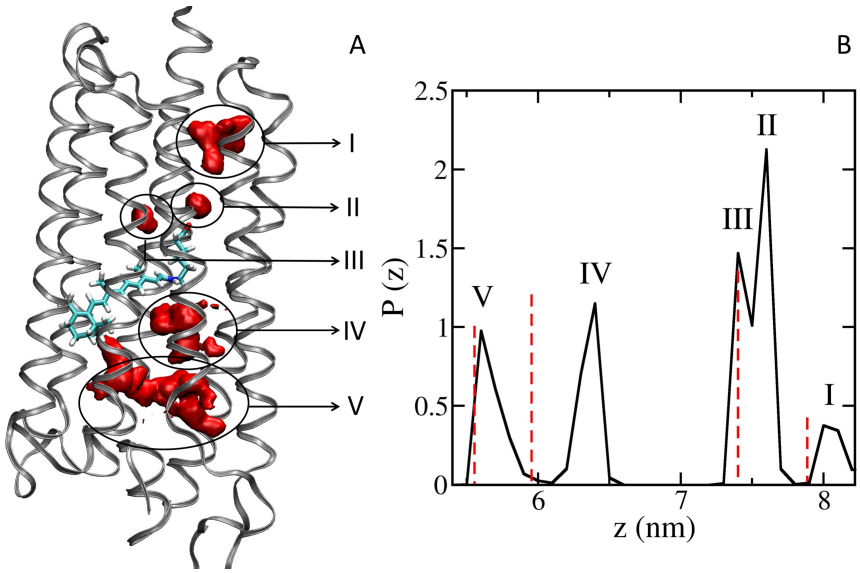

Figure 2: **Spatial localisation of water inside KR2 rhodopsin in the dark state** (A) The spatial density map of water inside the channel is shown by red patches and distinct pockets/cavities are labeled from I to V. The cavities from I to III reside above the retinal chromophore towards the cytoplasmic side, whereas IV and V are below it towards the extracellular side. (B) The population density of water along the z-direction (membrane normal) confirms the existence of five distinct hydration sites along the channel. The vertical dashed lines represent the position of water molecules in the crystal structure.

The probability distribution of water molecules along the z-axis (perpendicular to the membrane plane) further demonstrates the localisation of water at five specific sites of the channel (Fig. 2B). This is consistent with the localisation of water molecules in the crystal structure[4] (red vertical lines in Fig. 2B) and recent experimental observations.[7,24] Based on the location of the cavities, we have labeled them from I to V from the intracellular (top) to the extracellular (bottom) side (Fig. 2A). While the cavities I, IV and V appear to be broad, the cavities II and III are significantly small in size. We observed that the cavity III contains only one water molecule during the $1\mu s$ simulation time, whereas the number

of water inside the cavity II fluctuates between 1-2. Consistent with the earlier studies, we have observed a separation of water cluster by 6 Å at the vicinity of the retinal.[19,50]

Hydration level of the cavities

The average number of water molecules within the first hydration shell (coordination number) of a water in bulk is 4.5 (Fig. 3).[49] The surface of a biomolecule is expected to have reduced number of water in the first hydration shell due to the limited accessibility imposed by the biomolecule. This number should vary significantly for water molecules inside a cavity depending on the size of the cavity, i.e. the amount of water present in it. In KR2 rhodopsin, all the cavities identified in our study have severely reduced coordination number suggesting reduced hydration level inside the cavity.

For all the cavities except II and III, we find that the average number of water molecules within the first hydration shell is between 1-2. For cavities II and III this number is $\sim$0. Thus, the overall the hydration level of water inside rhodopsin channel is significantly compromised due to the confinement.

Although the hydration level in the cavity is compromised, the number of hydrogen bonding partners (including both water and protein residues) remains comparable to that of bulk water for all the cavities except cavity III (Fig. 4). The average number of hydrogen bonds in these cavities is ~ 3 compared to ~ 3.5 in case of bulk water. Hence, the energetic penalty due to desolvation can be to some extent compensated by making additional hydrogen bonding interactions with the surrounding amino-acid residues. But for cavity III, the average number of hydrogen bond is ~ 2. Thus, for cavity III, not only hydration level, but also the number of hydrogen bonding partners is significantly low.

Heterogeneity in the water-protein interaction energy within cavity

The interaction energy of the water molecules in the cavities I-III with the protein shows normal distribution indicating homogeneous environment in energy space (Fig. 5). On the

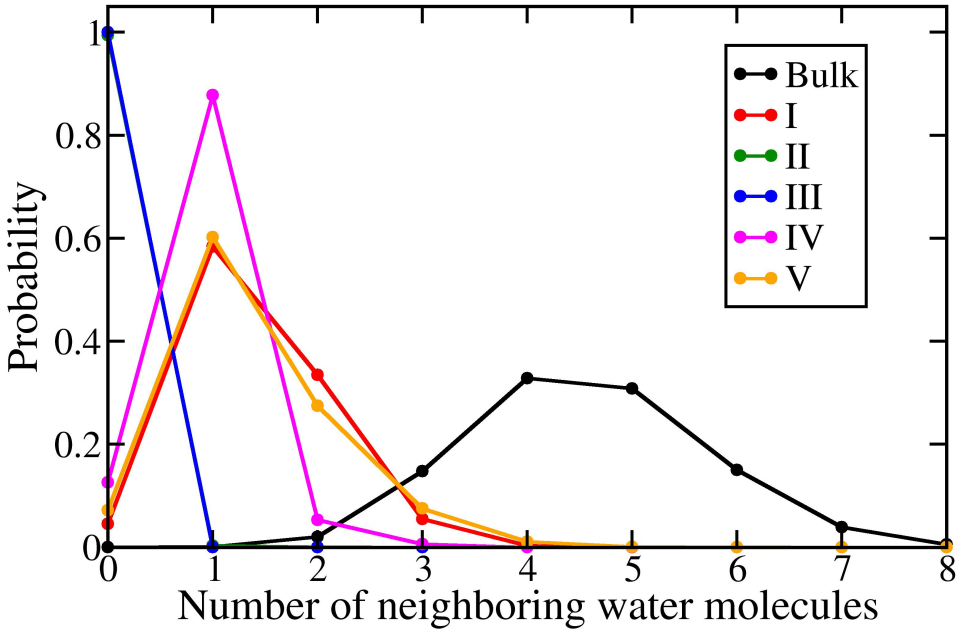

Figure 3: **Distribution of the number of neighboring water molecules around each water in different cavities inside the channel in comparison to the bulk water.** The probability distributions of the trapped water molecules show a drastic depletion in the number of neighboring water in the first hydration shell (radius 3 Å) compared to that of bulk water indicating reduced hydration. Interestingly, the water molecule in the cavity III does not have any neighboring water.

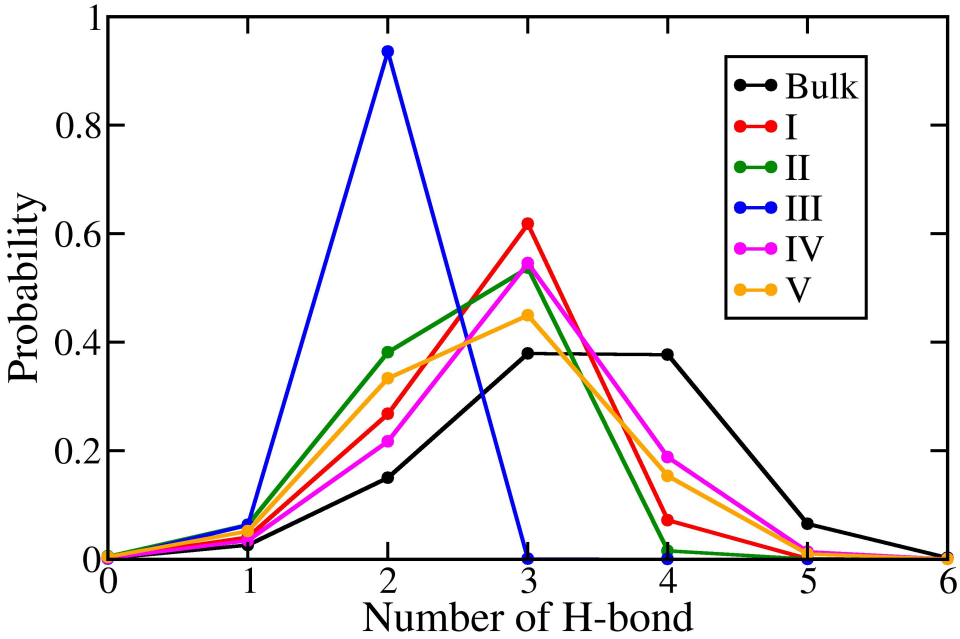

Figure 4: **Distributions of number of hydrogen bond with neighboring partners (both water and amino-acid residues) for water molecules in each of the cavities.** The probability distributions of the number of hydrogen bonds for the trapped water molecules are similar to that of the bulk water except those in the cavity II which show significantly less number of hydrogen bonds.

contrary, the water molecules in the cavities IV and V display a broad distribution in energy suggesting a heterogeneous environment. The probability distribution of the water molecules in the cavity V shows a long tail in the high stability region. Interestingly, in case of cavity IV, the distribution shows three distinct peaks (labeled as A, B and C in Fig. 5). These peaks are observed to be associated to three different environments as described below.

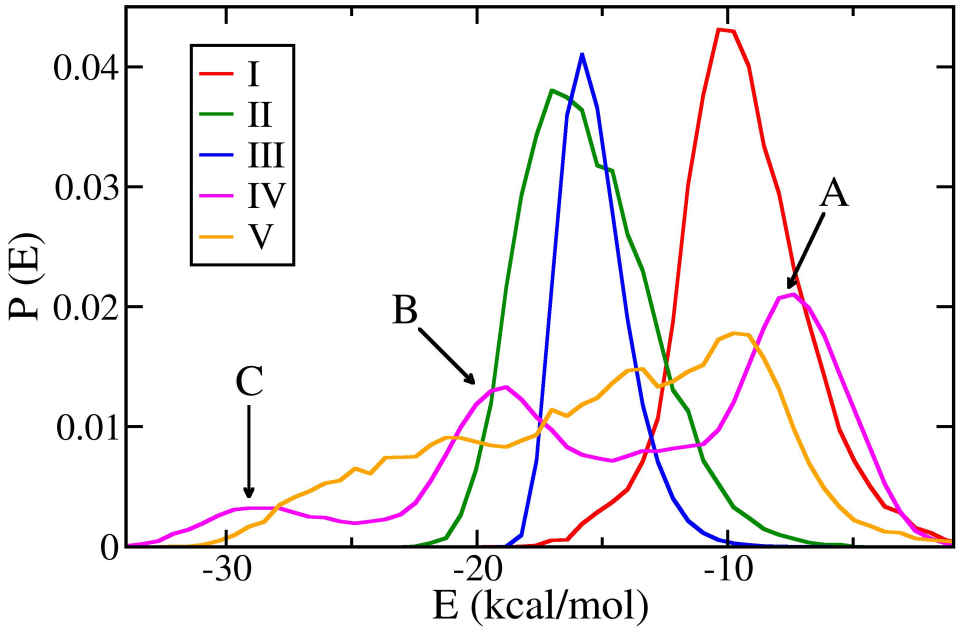

Figure 5: **Distribution of interaction energy of trapped water molecules with the neighboring amino-acid residues.** The water molecules inside the cavities situated above the retinal chromophore (cavities I-III) show a Gaussian distribution in the interaction energy suggesting homogeneous environments in terms of interaction with its environment. On the contrary, the water molecules trapped in the cavities situated below the chromophore (cavities IV and V) show a broad non-Gaussian distribution indicating heterogeneous environment. Interestingly, the water in the cavity IV shows three distinct peaks (labeled as A, B and C).

Deviation of several local properties of trapped water molecules from that of bulk water as discussed above clearly indicates that the local environment of these water molecules is expected to be different from that of bulk. Fig. 6 shows the local environments of water molecules in each of the cavities identified in our study.

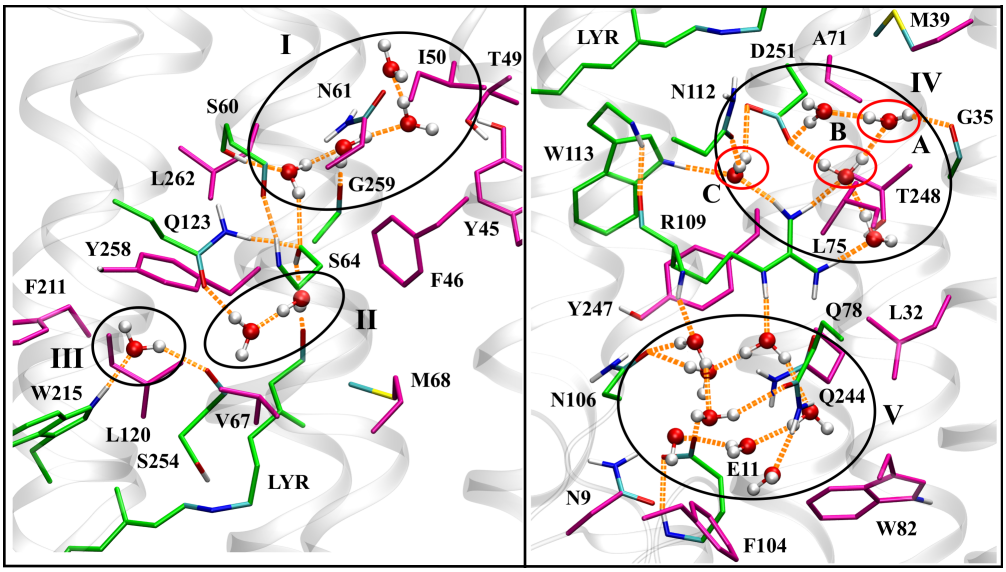

Figure 6: **Local environments of the water molecules trapped in each of the cavities.** Left panel: The water molecules trapped in the top part (above retinal) of rhodopsin (cavities I, II and III). The water molecules in cavity I show a string of hydrogen bonded network. The water molecules in cavity II are surrounded by S64, Q123 and LYR (Lysine attached to retinal) and are stabilised by formation of hydrogen bonds. The water trapped in the cavity III is surrounded by Y258, F211, W215 and S254. It forms strong H-bonds with W215 and S254. Right panel: The water molecules those are trapped in the bottom part of rhodopsin (cavities IV and V). The cavity IV is large in size and it accommodates multiple water molecules. The cavity is heterogeneous in terms of interaction between water and neighboring residues (see Fig.5). We have identified three local environments labeled as A, B and C. The cavity V resides at the exit part of the channel and it is connected to the bulk water. It contains several water molecules surrounded by key residues listed in Table 1.

The cavity I contains a string of water molecules formed via hydrogen bond (Fig. 6). A similar structure has been observed earlier in bacteriorhodopsin.[66] The cavity I is surrounded by key residues T49, I50, S60, N61, S64 and G259 (see Table 1). It is in the cytoplasmic side and the water in this cavity is easily exchanged with the cytoplasmic water. The location of this cavity is consistent with the ion-uptake cavity (IUC) identified in the crystal structures.[24]

The cavity II is constituted by F46, S64, Q123, LYR255 and Y258 and is situated below the cavity I (Fig. 6). The water in this cavity is stabilized by formation of hydrogen bonds with S64, Q123 and LYR255. Although the Fig. 6 shows two water molecules in this cavity, our whole MD trajectory shows occasional presence of a single water. Thus, the number of water in the cavity II fluctuates between 1-2.

The cavity III resides off-pathway from the main channel and is surrounded by F211, W215, Y258 and S254. The water in this cavity forms two hydrogen bonds with amino acid residues S254 and W215. Cavity III contains only one water molecule. Interestingly, this water is very strongly bound and remains in the cavity for the entire duration of 1.5 μs MD trajectory as will be demonstrated later.

The cavity IV is much bigger in size and therefore it contains multiple water molecules. Consistent with the energetic heterogeneity as shown in Fig. 5 there are three distinct local environments (Fig. 6, right panel). The labeling of water molecules is in accordance with the labels in Fig. 5. The three types of water molecules have following hydrogen bond partners: (i) water in region A forms hydrogen bond to the backbone of G35; (ii) water in B shares hydrogen bonds with two neighboring amino acid residues D251 and R109 and (iii) that in region C forms four hydrogen bonds with R109, N112, W113 and D251. Thus, the number of amino-acid partners increases from A to C consistent with the interaction energy distribution as shown in Fig. 5.

The cavity V resides at the exit of extracellular side. This is more like a channel containing several water molecules having diverse local environments. Some of the residues that form this cavity are listed in Table 1.

Table 1: List of amino-acid residues surrounding the cavities

Cavity	Surrounding residues
I	Y45, T49, I50, S60, N61, S64, G259
II	F46, S64, V67, Q123, LYR255, Y258
III	L120, F211, W215, S254, Y258
IV	G35, M39, A71, L75, R109, N112, W113, Y247, T248, D251
V	N9, E11, N12, L32, Q78, R109, Q157, E160, Q244, Y247, W82, F104

Residence time distribution in the cavities

As observed earlier, the water on a biological surface or inside cavity can stay for long enough time ranging from a few picoseconds to microseconds. In order to obtain the residence time of trapped water in different cavities, we have followed the z-coordinate of the O-atoms of the water molecules over time (Fig.7), where Z-axis is perpendicular to the membrane plane. The scattered dots above ane below the membrane bilayer signify the diffusive motion of the water molecules in the bulk phase. Occasionally they bind to the protein/membrane surface and get trapped into cavities (depicted by regions with z values fluctuating around a constant value with narrow width). The positions of the identified cavities are marked by horizontal dashed lines of same color.

We find a diverse range of residence time of trapped water molecules depending on the identity of cavity. The water molecules in cavity I dwell for relatively short period of time ranging from 1 to 10 ns. On the other hand, those in the cavities II, IV and V remain trapped for longer period of time (hundreds of nano-seconds). Surprisingly, the water in cavity III remains trapped during the entire simulation time scale of 1 μs! Thus, this cavity is very unique in nature. It does not contain any neighboring water molecule; remains in an isolated trapped environment and never gets exchanged with water in the other cavities. A similar experimental observation was reported earlier.[23] We speculate that this particular highly conserved water molecule may have a significant functional role during the photocycle

that is yet to be elucidated.

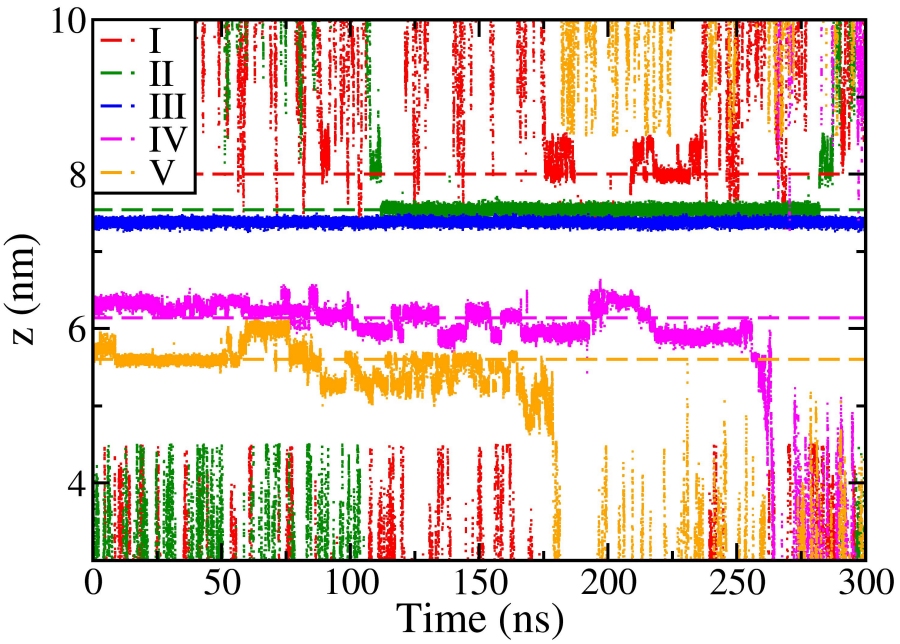

Figure 7: **The z-components of positions of few representative water molecules that are trapped inside the cavities.** The trapping events are evident from the reduced fluctuations in the z-values. The dashed lines represent average locations of respective cavities.

The time-series of the Z coordinate of the oxygen atoms of the water molecules (Fig. 7) provides us a way to quantify the residence time of all the water molecules that are trapped inside the cavities and thus we can gain a statistical information of mean residence time of water inside the cavities along with its probability distribution. Table 2 reports the average residence time of water molecules in each cavity. The averages were obtained over 500 water molecules. As the table suggests, the cavities near the membrane boundaries (I, II and V) are easily accessible to the bulk water and therefore they show relatively short mean residence time ranging from few nano-seconds to tens of nano-seconds. On the other hand, the water molecules in the relatively deeply buried cavity (IV) stay trapped for hundreds of nano-seconds. The water inside the cavity III never escapes out of the cavity within our

simulation timescale.

Each individual event of escape from a cavity is associated to a specific dwell time. Therefore, it is expected to have a unique value of residence time for each event of water entry into a given cavity. Fig. 8 shows the probability distribution of residence time of water in each cavity in logarithmic scale. The escape events are random as justified by the log-normal nature of the distributions. Note that log-normal distribution is ubiquitous in nature.[67] This is to note that an earlier study by Gracia *et al* in horse heart cytochrome c protein reports a power-law decay of probability with increasing residence time with the exponent value ranging from 0.4 to 1.8.[68]

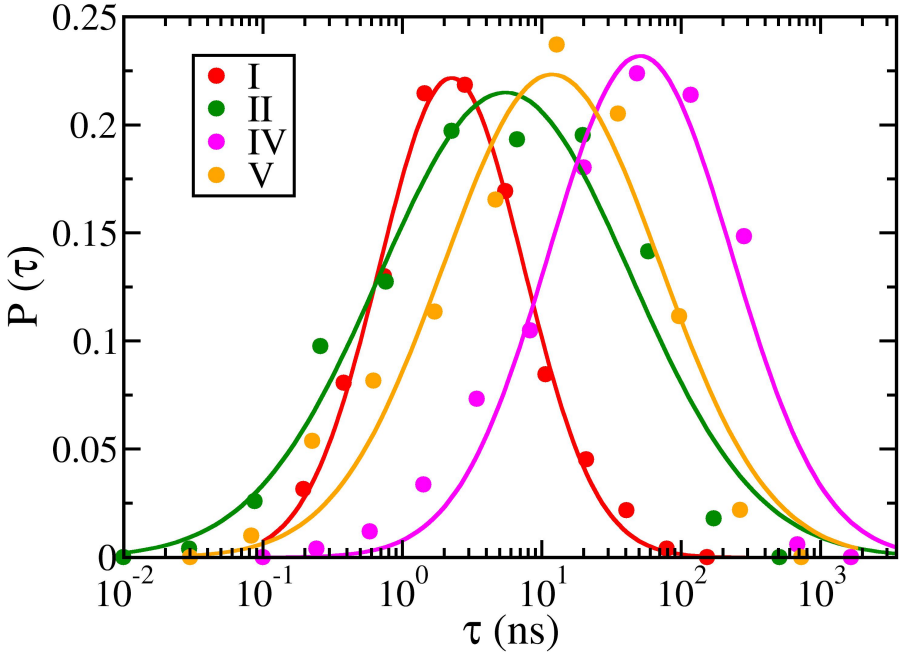

Figure 8: **Probability distribution of dwelling time of water molecules inside different cavities along the channel of KR2.** It shows a broad range of dwelling time starting from tens of picosecond to micro-second, consistent with the broad distribution of energy associated to the water molecules in different cavities as shown in Fig.5. The dwell times follow normal distribution suggesting random escape from the cavities. Each distribution contains 500 dwelling time data.

Table 2: List of average dwelling times and diffusion constants in different cavities including in bulk.

Cavity	τ (ns)	D (cm^2/s)
Bulk	-	3.3×10^{-4}
I	6.7	1.4×10^{-6}
II	28.5	8.9×10^{-8}
III	>1500	0
IV	132.3	2.2×10^{-7}
V	43.5	1.2×10^{-6}

Bottlenecks separating the cavities

The long residence times of each of the cavities is an evidence of presence of gateways in between the cavities. We find that the residues Q123 and S64 act as a gate in between cavities I and II consistent with earlier crystallographic studies.[7,24] The water molecules in I are in hydrogen bonded network. In order to escape and enter into II, they need to break hydrogen bonds in cavity I and then cross the bottleneck created by Q123 and S64. These two residues form hydrogen bonds with water molecules that try to escape I and enter II, thus create a gateway that prevents such transition. The residues S254, Y258 and W215 create an isolated environment for the water in cavity III. Furthermore, the strong hydrogen bonds formed by S254 and W215 with the water within such confined environment completely isolates the water. Therefore, water from cavity II cannot enter cavity III and vice versa. There is no exchange of water in between cavities II and IV as they are well separated by retinal (Fig. 2). The water in cavity II cannot reach retinal due to the presence of L120 and V67 that act as hydrophobic gate-keepers as observed in the previous study by Kaila and coworkers.[50] The cavities IV and V are separated by mainly R109 that controls the exchange of water in between them. Thus, overall the water exchange between cavities are controlled by few key amino-acid residues along the ion channel pathway.

Translational motion and diffusivity

The dynamics of a water strongly depends on its local environment. As we have observed the water molecules inside the rhodopsin channel are quite different from that in the bulk in terms of their local environment, their dynamics is expected to be different as well. To gain an insight about the translational motion, we have computed the mean square displacement (MSD) as a function of time for water in each cavity (Fig. 9). The water molecules in cavities I, IV and V show diffusive behavior within nanosecond as indicated by the linear increase of MSD with time. However, their diffusion constants are markedly low compared to that of bulk water (Table 2). In contrast, the water molecules in cavity II and III are non-diffusive in nature as indicated by saturation of MSD at long time. The MSD values at the saturation provide an approximate measure of cavity size. Thus, we obtain the cavity sizes for II and III to be ∼0.15 nm and ∼0.07 nm, respectively, that are smaller than the size of a water molecule (∼0.35 nm).

The environment of bulk water is homogeneous and identical for every water molecule. On the contrary, the environment of trapped water is different and each time a water enters a cavity it faces a different environment for the finite duration of time it stays inside the cavity. This is partly because of the dynamic nature of the amino-acid residues around the cavities. Therefore, each time a water enters a given cavity it may exhibit a different translational motion as observed from the time dependent mean square displacements (data not shown). At short time (¡1 ns), water molecules in all the cavities except that in cavity III show diffusive motion. We obtained short time diffusion constants of 500 trapped water molecules for each cavity from the slope of MSD vs. time plot within 1 ns. The diffusion constant largely varies with broad distribution as shown in Fig. 10. The log-normal distribution of diffusion constant follows Gaussian behavior and it shows a variation in three orders of magnitude ($\sim 10^{-9}$ to $\sim 10^{-6}$). This is to note that the water in the cavity III is non-diffusive in nature and therefore we have not computed the corresponding distribution.

While the translational motion of the water molecules within a cavity is diffusive in

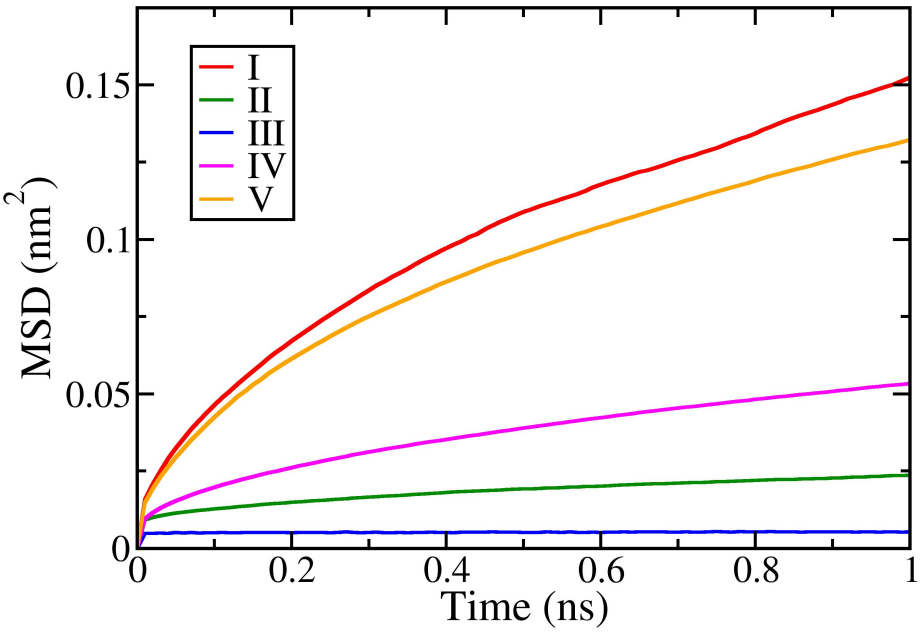

Figure 9: **The intra-cavity translational motion of water.** Mean square displacement (MSD) of water molecules inside the identified cavities is computed. It shows a diffusive motion at short time ($< 1ns$) as indicated by linear growth of MSD with time.

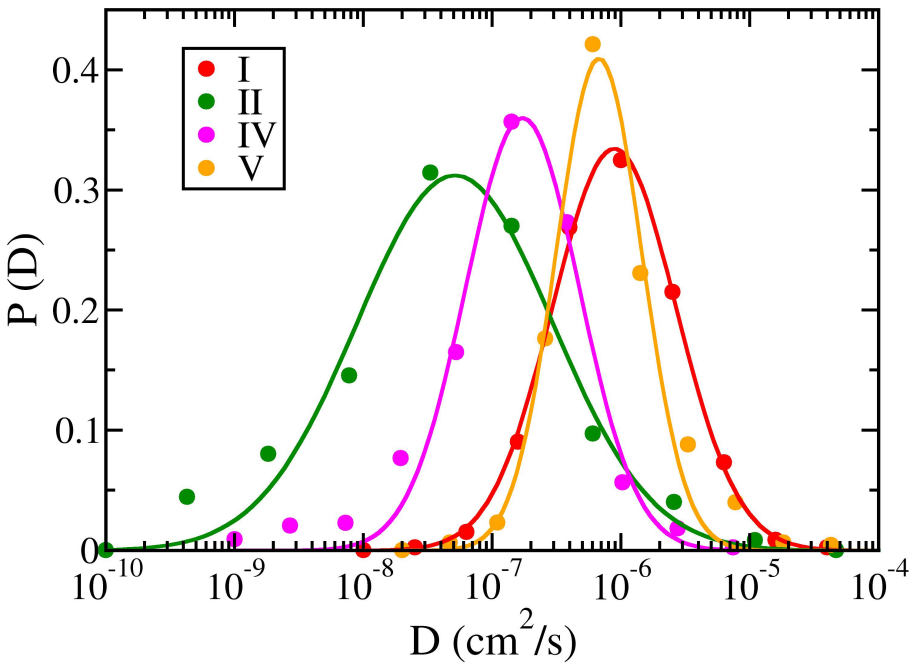

Figure 10: **Distribution of diffusion coefficient of water molecules trapped inside the cavities.** Diffusion coefficients were computed from the slope of the time dependent mean square displacement curves. Each distribution contains data from 500 water molecules.

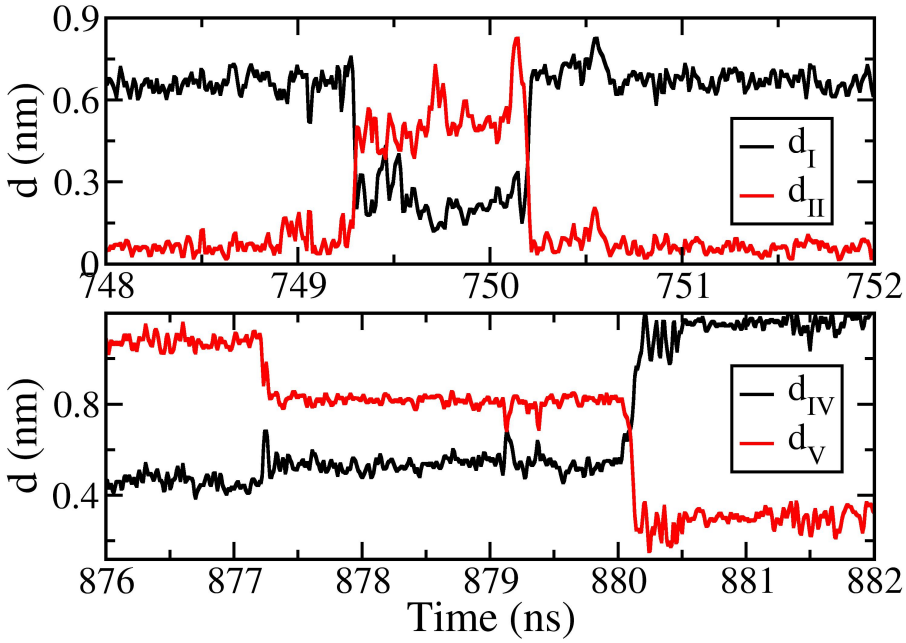

Figure 11: **The transitions of Water molecules in between cavities are observed to be through hopping motion.** The top panel shows the time evolution of distances of a representative water molecule from cavity I (black line, d_I) and II (red line, d_{II}). The bottom panel shows the distances of another representative water molecule from cavity IV (black line, d_{IV}) and V (red line, d_V).

nature, the inter-cavity transitions are observed to be through hopping motion as evident from the sharp changes in the distances of water molecules from the cavities involved in the transitions (Fig. 11).

Rotational dynamics

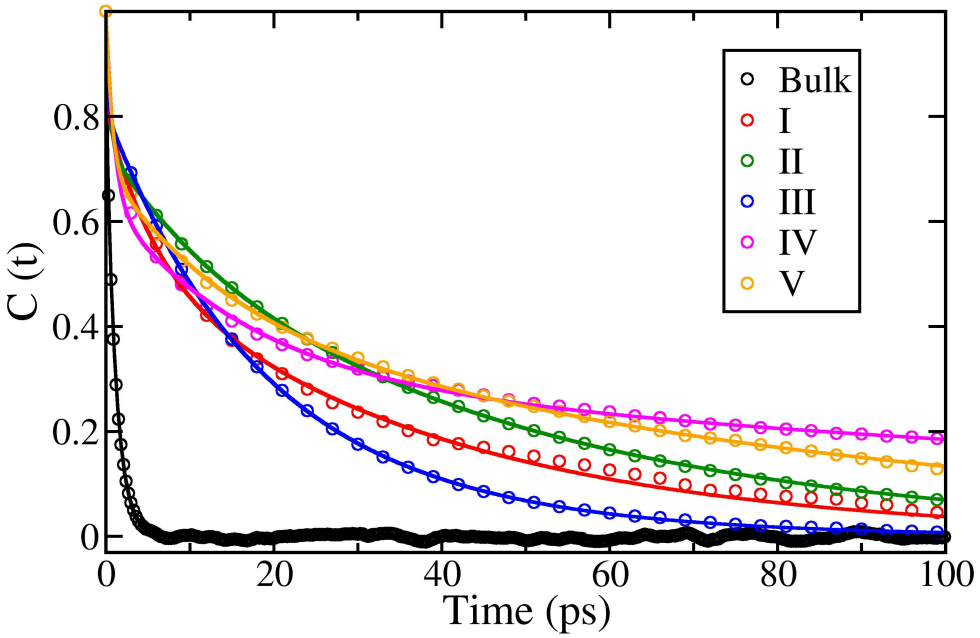

Figure 12: **Rotational dynamics of water molecules inside rhodopsin.** Rotational time correlation functions of trapped water molecules inside the cavities including the water in the bulk. The rotational relaxations in all the cavities are much slower (tens of picosecond) compared to that of bulk water (~ 1 ps). Note that the water in cavity III shows rotational relaxation time of similar range in comparison to the water molecules in the other cavities. This clearly indicates that the environment in cavity III does not impose any additional constraints on rotational motion despite of its hindered transnational motion.

The rotational motion of water depends on various factors. Confinement being one of them is expected to hinder its rotation. Water on bio-molecular surface with slow translational motion is associated with slow rotational dynamics. Thus, there is a coupling between translational and rotational motions. Consistent with this fact, the trapped water in the

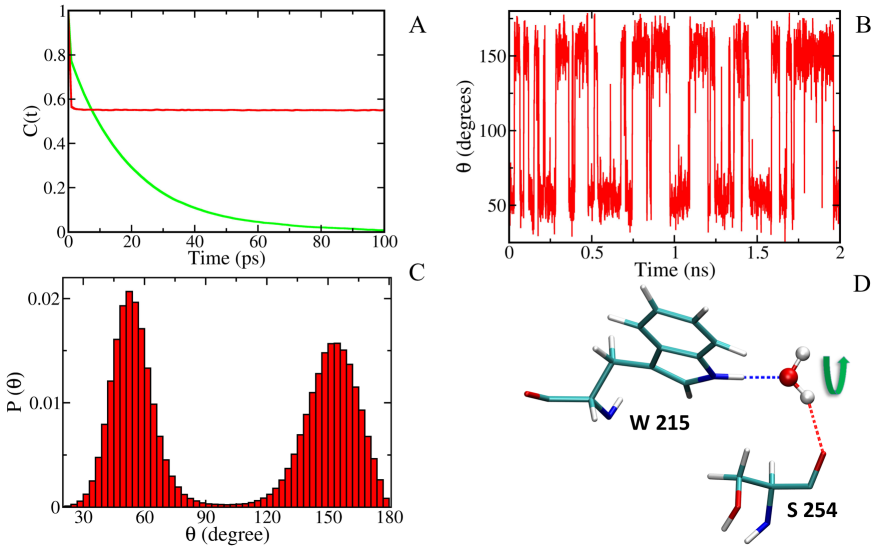

Figure 13: **The anisotropic rotational dynamics of water molecule trapped in the cavity III**.(A) Rotational time correlation functions of trapped water inside the cavity show that although the P_1 (first rank Legendre polynomial; green line) decays to 0, the P_2 (second rank Legendre polynomial; red line) does not decay to 0 rather it saturates at ~ 0.6 suggesting that the rotation is not completely free motion. (B) The time dependence of $O_w - H_w - O_{S254}$ angle shows frequent large fluctuations. (C) A bimodal distribution of the probability of the $O_w - H_w - O_{S254}$ angle is observed indicating presence of a bistable potential. (D) The local environment of the water molecule shows formation of two H-bonds with S254 and W215 residues. The water frequently rotates as depicted by the arrow by transiently breaking the H-bonds and then forming it again.

rhodopsin channel in general shows slower rotational dynamics compared to bulk water as is reflected in the slow decay of the first rank rotational time correlation function (Fig.12), where the correlation function is computed using following equation:

$$C(t) = \langle P_1(\vec{v}.\vec{v})\rangle; \text{ where } P_1(x) = x \tag{1}$$

where, P_1 is the first rank Legendre polynomial and $\vec{v}$ is the unit vector perpendicular to the water plane. We noticed that the rotational time correlation function decay is associated to multiple time scales. Therefore, we fitted the data with the following tri-exponential form to find out the time scales and their contributions to the overall rotational dynamics.

$$C(t) = w_0\ e^{-t/\tau_0} + w_1\ e^{-t/\tau_1} + w_2\ e^{-t/\tau_2} \tag{2}$$

where, w_0, w_1 and w_2 are the weight factors and τ_0, τ_1 and τ_2 are corresponding time constants. The best fit parameters are reported in Table 3.

The bulk water shows only two time scales in which the time constant 1.2 ps is the major contributor. In contrast, the trapped water shows three time constants: (i) the smallest time constant is in the range 0.1-1 ps, (ii) the intermediate one is in the range of ∼1-20 ps and (iii) the largest time constant is of the order of hundreds of picoseconds. The largest time scale is expected to be associated to the confinement and the interaction of water with surrounding amino acid residues which are absent in the case of bulk water. Interestingly, the slowest time scales for cavities IV and V (below the retinal) are much larger than that of the cavities I-III (above the retinal) which suggests that the water at the upper part of retinal in the resting state are rotationally more flexible than the bottom counterpart. The observation of having faster rotational time scale for cavities II and III compared to that of IV and V is in contrast with the translational dynamics. Even though the water molecules in cavities II and III are translationally trapped their rotational dynamics is relatively faster compared to that in the cavities IV and V. Overall, we find a multi-exponential decay of rotational

correlation function and the decay time is much slower than that of the bulk water.

We find a unique rotational dynamics for the water in cavity III. The first rank rotational correlation function (Eq.1) of the vector perpendicular to water plane decays to zero. We computed the second rank rotational correlation function using following equation:

$$C(t) = \langle P_2(\vec{v}.\vec{v})\rangle; \text{ where } P_2(x) = \frac{1}{2}(3x^2 - 1) \tag{3}$$

where, P_2 is the second rank Legendre polynomial and $\vec{v}$ is the unit vector of concern. Interestingly, it does not fully decay to zero. Rather it saturates to ∼0.6 at long time (Fig.13A). This suggests that the rotation is not a free motion. In order to investigate the reason behind it, we computed the time dependent $O_w - H_w - O_{S254}$ angle and it reveals a frequent large rotational jump motion (Fig. 13B). The probability distribution of this angle appears to be bimodal in nature (Fig. 13C). The local configuration corresponding to the most probable angle is shown in Fig. 13D. The flipping of the water molecule gives rise to the other most probable angle. Thus, the rotational motion of the water in the cavity III is highly restricted. It undergoes occasional flip motion in a specific direction.

Table 3: Rotational time scales (time constants are in picosecond)

Cavity	w_0	w_1	w_2	τ_0	τ_1	τ_2
Bulk	0.18	0.82	-	0.1	1.2	-
I	0.19	0.28	0.53	0.1	5.5	38
II	0.25	0.15	0.6	0.4	11.8	47
III	0.19	0.58	0.23	0.2	17.1	28
IV	0.36	0.34	0.3	1.0	16.7	204
V	0.3	0.27	0.43	0.7	14.2	85

Rotational anisotropy

Although the translational motion of a water in the bulk is isotropic in nature, the rotational motion as shown in Fig. 14 is observed to be slightly anisotropic (I_A=2, where I_A is the ratio of the largest and the smallest rotational timescales among the three rotational correlation

functions computed for three orthogonal vectors: dipole moment of water, orthogonal to the dipole moment vector within the water plane and the vector orthogonal to the water plane). This is consistent with the earlier study by Ropp *et al.*[69] Since each of the three rotational correlation functions is multi-exponential in nature, we have obtained the effective time scale for each of them using following equation:

$$\tau = \frac{\int_0^\infty dt\ t\ C(t)}{\int_0^\infty dt\ C(t)} \tag{4}$$

The rotational motion of water on biological surface is slowed down compared to that in the bulk.[30,70–72] We find a similar slowing down for the water molecules inside cavity. In addition, we observed that the rotational motion inside protein cavity is highly anisotropic with the rotation of the dipole moment vector being the slowest among all the three orthogonal vectors (Fig. 14). The anisotropy indices of water molecules in the cavities I and V are 11 and 14, respectively (see Table 4). The rotational dynamics is more anisotropic as one moves towards the core of the protein. The water molecules in the core cavities II and IV show anisotropy indices 40 and 24, respectively. On the other hand, the water in the cavity III is extremely anisotropic in nature with observed anisotropy index $\sim 10^{12}$.

Table 4: Rotational time scales of three mutually orthogonal vectors and rotational anisotropicity. Time constants are in picosecond.

Cavity	τ_{HH}	τ_{μ}	$\tau_{\perp}$	I_A
Bulk	15.03	21.3	10.4	2
I	42.83	544.93	37.74	14
II	52.54	1715.68	42.23	40
III	15.41	5.17×10^{13}	15.41	3.35×10^{12}
IV	64.44	1266.04	53.45	24
V	80.59	902.82	90.72	11

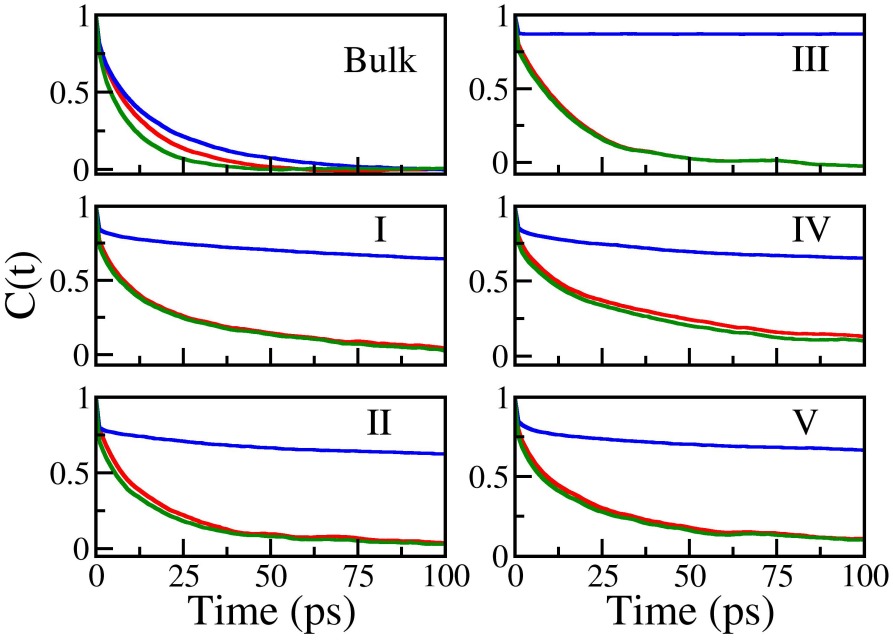

Figure 14: **Rotational time correlation functions of trapped water molecules inside the cavities including the water in the bulk for three mutually orthogonal vectors.** The black, red and green lines represent rotational correlation function of the vectors corresponding to H-H bond, dipole moment of the molecule and the perpendicular direction to the plane of the molecule, respectively.

Conclusion

We have carried out an extensive all-atom molecular dynamics simulation to explore the structure and dynamics of water inside rhodopsin (KR2) channel in the dark state. Our study reveals five specific regions where the water molecules are trapped for significantly long time. These regions/cavities are spatially disjoint indicating the presence of protein side-chains acting as gateways controlling the movement of water between these cavities.

The cytoplasmic side (above the retinal chromophore) possesses three distinct cavities (I, II and III) whereas the extracellular side contains two cavities (IV and V). Cavity I is well connected to the cytoplasm and there is rapid exchange of water molecules. Multiple water molecules are accommodated in this cavity and they form a string like extended hydrogen bond network. The cavity II, located below the cavity I and well separated from it, can accommodate up to two water molecules. The cavity III is located off-pathway from the rhodopsin channel and it carries strictly one water molecule. The cavities IV and V accommodate several water molecules.

The local structure and dynamics of these water molecules demonstrate significant heterogeneity. In all the cavities, the number of water in first hydration shell is significantly less compared to that in the bulk water. On the contrary, except the water in the cavity III, the number of hydrogen bond in all other cavities remains similar to that of the bulk water due to the compensation made by the formation of water-protein hydrogen bonds. The water-protein interaction energy is highly heterogeneous indicated by the non-Gaussian nature of the energy distribution. The cavity IV contains three distinct sites, which is reflected in the appearance of three peaks in the energy distribution.

The observed residence time of trapped water varies from few nanoseconds to hundreds of nanoseconds depending on the identity of the cavity. Interestingly, the water inside cavity III never escapes in our 1 μS simulation time. The residence time follows a log-normal distribution.

The translational motion of the trapped water is diffusive in nature within 1 ns but is

markedly slowed down compared to the bulk. Water molecules in the cavities II and III seize to diffuse within 1 ns. Although the water molecules diffuse within the cavities, the exchange of water in between cavities is rare and it occurs through hopping motion controlled by the protein sidechains acting as gateways.

The rotational dynamics also gets hindered significantly as compared to that of bulk water. The rotational relaxation is multi-exponential in nature. The slowest component of the decay is of the order of hundreds of picoseconds as compared to ∼1 picosecond in case of bulk water. Thus, the rotational dynamics of trapped water is slowed down by a factor of ∼100. Water in the cavity III depicts a unique flipping motion between two distinct orientations with possible functional significance. We find the rotation of the trapped water molecules to be highly anisotropic in nature. The results presented in this study lay the groundwork for understanding the intimate role that hydration might play in the sodium-pumping mechanism of KR2 rhodopsin. While this work focuses exclusively on the water structure and dynamics in the resting state of KR2 rhodopsin, future work will further explore the coupling between the water and protein dynamics, and their effects on the various stages of the overall photocycle.

Acknowledgement

SC thanks SERB/DST, India for funding (ECR/2018/002903). Authors thank SNBNCBS, Kolkata for the supercomputing facility. We thank Dr. Debashree Ghosh and Dr. Surya Kanta Ghosh for several insightful discussions and valuable suggestions on the manuscript.

References

(1) Gushchin, I.; Gordeliy, V. *Membrane Protein Complexes: Structure and Function*; Springer: Singapore, 2018; Vol. 87; pp 19–56.

(2) Kandori, H.; Inoue, K.; Tsunoda, S. P. Light-Driven Sodium-Pumping Rhodopsin: A New Concept of Active Transport. *Chem. Rev.* **2018**, *118*, 10646–10658.

(3) Inoue, K.; Ono, H.; Abe-Yoshizumi, R.; Yoshizawa, S.; Ito, H.; Kogure, K.; Kandori, H. A light-driven sodium ion pump in marine bacteria. *Nat. Commun.* **2013**, *4*, 1678–.

(4) Kato, H. E. et al. Structural basis for Na+ transport mechanism by a light-driven Na^+ pump. *Nature* **2015**, *521*, 48–53.

(5) Gushchin, I. et al. Crystal structure of a light-driven sodium pump. *Nat. Struct. Mol. Biol.* **2015**, *22*, 390–395.

(6) Skopintsev, P. et al. Femtosecond-to-millisecond structural changes in a light-driven sodium pump. *Nature* **2020**, *583*, 314–318.

(7) Kovalev, K.; Polovinkin, V.; Gushchin, I.; Alekseev, A.; Shevchenko, V.; Borshchevskiy, V.; Astashkin, R.; Balandin, T.; Bratanov, D.; Vaganova, S.; Popov, A.; Chupin, V.; Buldt, G.; Bamberg, E.; Gordeliy, V. Structure and mechanisms of sodium-pumping KR2 rhodopsin. *Sci. Adv.* **2019**, *5*, eaav2671.

(8) Ernst, O. P.; Lodowski, D. T.; Elstner, M.; Hegemann, P.; Brown, L. S.; Kandori, H. Microbial and Animal Rhodopsins: Structures, Functions, and Molecular Mechanisms. *Chem. Rev.* **2014**, *114*, 126–163.

(9) Abe-Yoshizumi, R.; Inoue, K.; Kato, H. E.; Nureki, O.; Kandori, H. Role of Asn112 in a Light-Driven Sodium Ion-Pumping Rhodopsin. *Biochemistry* **2016**, *55*, 5790–5797.

(10) Shevchenko, V.; Gushchin, I.; Polovinkin, V.; Kovalev, K.; Balandin, T.; Borshchevskiy, V.; Gordeliy, V. *Optogenetics: From Neuronal Function to Mapping and Disease Biology*; Cambridge University Press, 2017; pp 79–92.

(11) Gerwert, K.; Freier, E.; Wolf, S. The role of protein-bound water molecules in microbial rhodopsins. *Biochim. Biophys. Acta - Bioenerg.* **2014**, *1837*, 606–613.

(12) Oesterhelt, D.; Stoeckenius, W. Rhodopsin-like Protein from the Purple Membrane of Halobacterium halobium. *Nat. New Biol.* **1971**, *233*, 149–152.

(13) Kato, Y.; Inoue, K.; Kandori, H. Kinetic Analysis of H^+-Na^+ Selectivity in a Light-Driven Na^+-Pumping Rhodopsin. *J. Phys. Chem. Lett.* **2015**, *6*, 5111–5115.

(14) Vogt, A.; Silapetere, A.; Grimm, C.; Heiser, F.; Möller, M. A.; Peter,; Hegemann, Engineered Passive Potassium Conductance in the KR2 Sodium Pump. *Biophys. J.* **2019**, *116*, 1941–1951.

(15) Nishimura, N.; Mizuno, M.; Kandori, H.; Mizutani, Y. Distortion and a Strong Hydrogen Bond in the Retinal Chromophore Enable Sodium-Ion Transport by the Sodium-Ion Pump KR2. *J. Phys. Chem. B* **2019**, *123*, 3430–3440.

(16) Bogachev, A. V.; Bertsova, Y. V.; Verkhovskaya, M. L.; Mamedov, M. D.; Skulachev, V. P. Real-time kinetics of electrogenic Na^+ transport by rhodopsin from the marine flavobacterium Dokdonia sp. PRO95. *Sci. Rep.* **2016**, *6*, 21397.

(17) Gushchin, I.; Shevchenko, V.; Polovinkin, V.; Borshchevskiy, V.; Buslaev, P.; Bamberg, E.; Gordeliy, V. Structure of the Light-Driven Sodium Pump KR2 and Its Implications for Optogenetics. *FEBS J.* **2016**, *283*, 1232–1238.

(18) Yuan, S.; Filipek, S.; Palczewski, K.; Vogel, H. Activation of G-protein-coupled receptors correlates with the formation of a continuous internal water pathway. *Nature Communications* **2014**, *5*, 4733.

(19) Ardevol, A.; Hummer, G. Retinal isomerization and water-pore formation in channelrhodopsin-2. *Proc. Natl. Acad. Sci., USA* **2018**, *115*, 3557–3562.

(20) Okada, T.; Fujiyoshi, Y.; Silow, M.; Navarro, J.; Landau, E. M.; Shichida, Y. Functional role of internal water molecules in rhodopsin revealed by x-ray crystallography. *Proc. Natl. Acad. Sci., USA* **2002**, *99*, 5982–5987.

(21) Ito, S.; Kato, H. E.; Taniguchi, R.; Iwata, T.; Nureki, O.; Kandori, H. Water-Containing Hydrogen-Bonding Network in the Active Center of Channelrhodopsin. *J. Am. Chem. Soc.* **2014**, *136*, 3475–3482.

(22) Venkatakrishnan, A. J.; Ma, A. K.; Fonseca, R.; Latorraca, N. R.; Kelly, B.; Betz, R. M.; Asawa, C.; Kobilka, B. K.; Dror, R. O. Diverse GPCRs exhibit conserved water networks for stabilization and activation. *Proceedings of the National Academy of Sciences* **2019**, *116*, 3288–3293.

(23) Angel, T. E.; Gupta, S.; Jastrzebska, B.; Palczewski, K.; Chance, M. R. Structural waters define a functional channel mediating activation of the GPCR, rhodopsin. *Proc. Natl. Aca. Sci. USA* **2009**, *106*, 34.

(24) Kovalev, K. et al. Molecular mechanism of light-driven sodium pumping. *Nat. Comm.* **2020**, *11*, 2137.

(25) Bagchi, B. *Water in Biological and Chemical Processes From Structure and Dynamics to Function*; Cambridge University Press, 2013.

(26) Bagchi, B. Untangling complex dynamics of biological water at protein–water interface. *Proc. Natl. Acad. Sci.* **2016**, *113*, 8355–8357.

(27) Ball, P. Water as an Active Constituent in Cell Biology. *Chem. Rev.* **2008**, *108*, 74–108.

(28) Laage, D.; Elsaesser, T.; Hynes, J. T. Water Dynamics in the Hydration Shells of Biomolecules. *Chem. Rev.* **2017**, *117*, 10694–10725.

(29) Frauenfelder, H.; Chen, G.; Berendzen, J.; Fenimore, P. W.; Jansson, H.; McMahon, B. H.; Stroe, I. R.; Swenson, J.; Young, R. D. A unified model of protein dynamics. *Proc. Natl. Acad. Sci.* **2009**, *106*, 5129–5134.

(30) Bagchi, B. Water Dynamics in the Hydration Layer around Proteins and Micelles. *Chem. Rev.* **2005**, *105*, 3197–3219.

(31) Zhang, L.; Wang, L.; Kao, Y.-T.; Qiu, W.; Yang, Y.; Okobiah, O.; Zhong, D. Mapping hydration dynamics around a protein surface. *Proc. Natl. Acad. Sci.* **2007**, *104*, 18461–18466.

(32) Rasaiah, J. C.; Garde, S.; Hummer, G. Water in Nonpolar Confinement: From Nanotubes to Proteins and Beyond. *Annu. Rev. Phys. Chem.* **2007**, *59*, 713–740.

(33) Zhong, D.; Pal, S. K.; Zewail, A. H. Biological water: A critique. *Chem. Phys. Lett.* **2011**, *503*, 1–11.

(34) Levy, Y.; Onuchic, J. N. Water mediation in protein folding and molecular recognition. *Annu. Rev. Biophys. Biomol. Struct.* **2006**, *35*, 389–415.

(35) Chaplin, M. Do we underestimate the importance of water in cell biology? *Nat. Rev. Mol. Cell Biol.* **2006**, *7*, 861–866.

(36) Leitner, D. M.; Hyeon, C.; Reid, K. M. Water-mediated biomolecular dynamics and allostery. *J. Chem. Phys.* **2020**, *152*, 240901.

(37) Luisi, B. F.; Xu, W. X.; Otwinowski, Z.; Freedman, L. P.; Yamamoto, K. R.; Sigler, P. B. Crystallographic analysis of the interaction of the glucocorticoid receptor with DNA. *Nature* **1991**, *352*, 497–505.

(38) Robinson, C. R.; Sligar, S. G. Molecular recognition mediated by bound water: A mechanism for star activity of the restriction endonuclease EcoRI. *J. Mol. Biol.* **1993**, *234*, 302–306.

(39) Robinson, C. R.; Sligar, S. G. Changes in solvation during DNA binding and cleavage are critical to altered specificity of the EcoRI endonuclease. *Proc. Natl. Acad. Sci., USA* **1998**, *95*, 2186–2191.

(40) Pal, S. K.; Peon, J.; Bagchi, B.; Zewail, A. H. Biological Water: Femtosecond Dynamics of Macromolecular Hydration. *J. Phys. Chem. B* **2002**, *106*, 12376–12395.

(41) Bhattacharyya, S. M.; Wang, Z.-G.; Zewail, A. H. Dynamics of Water near a Protein Surface. *J. Phys. Chem. B* **2003**, *107*, 13218–13228.

(42) Nandi, N.; Bagchi, B. Dielectric Relaxation of Biological Water. *J. Phys. Chem. B* **1997**, *101*, 10954–10961.

(43) Otting, G.; Liepinsh, E.; Wuthrich, K. Protein hydration in aqueous solution. *Science* **1991**, *254*, 974–980.

(44) Svergun, D. I.; Richard, S.; Koch, M. H. J.; Sayers, Z.; Kuprin, S.; Zaccai, G. Protein hydration in solution: Experimental observation by x-ray and neutron scattering. *Proc. Natl. Acad. Sci. U. S. A.* **1998**, *95*, 2267–2272.

(45) Hande, V. R.; Chakrabarty, S. Structural Order of Water Molecules around Hydrophobic Solutes: Length-Scale Dependence and Solute-Solvent Coupling. *J. Phys. Chem. B* **2015**, *119*, 11346–11357.

(46) Hande, V. R.; Chakrabarty, S. Exploration of the presence of bulk-like water in AOT reverse micelles and water-in-oil nanodroplets: the role of charged interfaces, confinement size and properties of water. *Phys. Chem. Chem. Phys.* **2016**, *18*, 21767–21779.

(47) Denisov, V. P.; Peters, J.; Hörlein, H. D.; Halle, B. Using buried water molecules to explore the energy landscape of proteins. *Nat. Struct. Mol. Biol.* **1996**, *3*, 505–509.

(48) Ernst, J. A.; Clubb, R. T.; Zhou, H.-X.; Gronenborn, A. M.; Clore, G. M. Demonstration of positionally disordered water within a protein hydrophobic cavity by NMR. *Science* **1995**, *267*, 1813–1817.

(49) García, A. E.; Hummer, G. Water Penetration and Escape in Proteins. *PROTEINS: Struct. Func. Genet.* **2000**, *38*, 261–272.

(50) Suomivuori, C.-M.; Gamiz-Hernandez, A. P.; Sundholm, D.; Kaila, V. R. I. Energetics

and dynamics of a light-driven sodium-pumping rhodopsin. *Proc. Natl. Acad. Sci., USA* **2017**, *114*, 7043–7048.

(51) Hussain, S.; Franck, J. M.; Han, S. Transmembrane Protein Activation Refined by Site-Specific Hydration Dynamics. *Angew. Chemie Intl. Ed.* **2013**, *52*, 1953–1958.

(52) Bondar, A.-N.; Baudry, J.; Suhai, S.; Fischer, S.; Smith, J. C. Key Role of Active-Site Water Molecules in Bacteriorhodopsin Proton-Transfer Reactions. *J. Phys. Chem. B* **2008**, *112*, 14729–14741.

(53) Feng, J.; Mertz, B. Proteorhodopsin Activation Is Modulated by Dynamic Changes in Internal Hydration. *Biochemistry* **2015**, *54*, 7132–7141.

(54) Boyden, E. S.; Zhang, F.; Bamberg, E.; Nagel, G.; Deisseroth, K. Millisecond-timescale, genetically targeted optical control of neural activity. *Nat. Neuro.* **2005**, *8*, 1263–1268.

(55) Hoque, M. R.; Ishizuka, T.; Inoue, K.; Abe-Yoshizumi, R.; Igarashi, H.; Mishima, T.; Kandori, H.; Yawo, H. A Chimera Na^+-Pump Rhodopsin as an Effective Optogenetic Silencer. *Plos One* **2016**, *11*, e0166820.

(56) Abraham, M. J.; Murtola, T.; Schulz, R.; Páll, S.; Smith, J. C.; Hess, B.; Lindahl, E. GROMACS: High performance molecular simulations through multi-level parallelism from laptops to supercomputers. *SoftwareX* **2015**, *1-2*, 19 – 25.

(57) Jo, S.; Kim, T.; Iyer, V. G.; Im, W. CHARMM-GUI: A Web-Based Graphical User Interface for CHARMM. *J. Comput. Chem.* **2008**, *29*, 1859–65.

(58) Bussi, G.; Donadio, D.; Parrinello, M. Canonical sampling through velocity rescaling. *The Journal of Chemical Physics* **2007**, *126*, 014101.

(59) Parrinello, M.; Rahman, A. Polymorphic transitions in single crystals: A new molecular dynamics method. *Journal of Applied Physics* **1981**, *52*, 7182–7190.

(60) Best, R. B.; Zhu, X.; Shim, J.; Lopes, P. E. M.; Mittal, J.; Feig, M.; MacKerell Jr, A. D. Optimization of the Additive CHARMM All-Atom Protein Force Field Targeting Improved Sampling of the Backbone ϕ, ψ and Side-Chain $\chi(1)$ and $\chi(2)$ Dihedral Angles. *J. Chem. Theor. Comput.* **2012**, *8*, 3257–3273.

(61) Nina, M.; Roux, B.; Smith, J. C. Functional interactions in bacteriorhodopsin: a theoretical analysis of retinal hydrogen bonding with water. *Biophys. J.* **1995**, *68*, 25–39.

(62) Tajkhorshid, E.; Paizs, B.; Suhai, S. Conformational Effects on the Proton Affinity of the Schiff Base in Bacteriorhodopsin: A Density Functional Study. *J. Phys. Chem. B* **1997**, *101*, 8021–8028.

(63) Tajkhorshid, E.; Suhai, S. Influence of the Methyl Groups on the Structure, Charge Distribution, and Proton Affinity of the Retinal Schiff Base. *J. Phys. Chem. B* **1999**, *103*, 5581–5590.

(64) Hayashi, S.; Ohmine, I. Proton Transfer in Bacteriorhodopsin: Structure, Excitation, IR Spectra, and Potential Energy Surface Analyses by an ab Initio QM/MM Method. *J. Phys. Chem. B* **2000**, *104*, 10678–10691.

(65) Hayashi, S.; Tajkhorshid, E.; Pebay-Peyroula, E.; Royant, A.; Landau, E. M.; Navarro, J.; Schulten, K. Structural Determinants of Spectral Tuning in Retinal Proteins - Bacteriorhodopsin vs Sensory Rhodopsin II. *J. Phys. Chem. B* **2001**, *105*, 10124–10131.

(66) Mathias, G.; Marx, D. Structures and spectral signatures of protonated water networks in bacteriorhodopsin. *Proc. Natl. Acad. Sci. USA* **2007**, *104*, 6980–6985.

(67) Limpert, E.; Stahel, W. A.; Abbt, M. Log-normal Distributions across the Sciences: Keys and Clues: On the charms of statistics, and how mechanical models resembling gambling machines offer a link to a handy way to characterize log-normal distributions,

which can provide deeper insight into variability and probability—normal or log-normal: That is the question. *Bioscience* **2001**, *51*, 341–352.

(68) García, A. E.; Hummer, G. Conformational dynamics of cytochrome c: Correlation to hydrogen exchange. *Proteins: Structure, Function, and Bioinformatics* **1999**, *36*, 175–191.

(69) Ropp, J.; Lawrence, C.; Farrar, T. C.; Skinner, J. L. Rotational Motion in Liquid Water Is Anisotropic: A Nuclear Magnetic Resonance and Molecular Dynamics Simulation Study. *J. Am. Chem. Soc.* **2001**, *123*, 8047–8052.

(70) Mukherjee, S.; Mondal, S.; Bagchi, B. Distinguishing dynamical features of water inside protein hydration layer: Distribution reveals what is hidden behind the average. *J. Chem. Phys.* **2017**, *147*, 024901.

(71) Persson, F.; Söderhjelm, P.; Halle, B. How proteins modify water dynamics. *J. Chem. Phys.* **2018**, *148*, 215103.

(72) Braun, D.; Schmollngruber, M.; Steinhauser, O. Rotational dynamics of water molecules near biological surfaces with implications for nuclear quadrupole relaxation. *Phys. Chem. Chem. Phys.* **2016**, *18*, 24620–24630.